Since January 2020 Elsevier has created a COVID-19 resource centre with free information in English and Mandarin on the novel coronavirus COVID-19. The COVID-19 resource centre is hosted on Elsevier Connect, the company's public news and information website.

CHEST

Feasibility of a 5G-Based Robot-Assisted Remote Ultrasound System for Cardiopulmonary Assessment of Patients With Coronavirus Disease 2019

Ruizhong Ye, MD; Xianlong Zhou, MD; Fei Shao, MD; Linfei Xiong, PhD; Jun Hong, MD; Haijun Huang, MD; Weiwei Tong, PhD; Jing Wang, MD; Shuangxi Chen, MD; Ailin Cui, MD; Chengzhong Peng, MD; Yan Zhao, MD; and Legao Chen, MD

BACKGROUND: Traditional methods for cardiopulmonary assessment of patients with coronavirus disease 2019 (COVID-19) pose risks to both patients and examiners. This necessitates a remote examination of such patients without sacrificing information quality.

RESEARCH QUESTION: The goal of this study was to assess the feasibility of a 5G-based robot-assisted remote ultrasound system in examining patients with COVID-19 and to establish an examination protocol for telerobotic ultrasound scanning.

STUDY DESIGN AND METHODS: Twenty-three patients with COVID-19 were included and divided into two groups. Twelve were nonsevere cases, and 11 were severe cases. All patients underwent a 5G-based robot-assisted remote ultrasound system examination of the lungs and heart following an established protocol. Distribution characteristics and morphology of the lung and surrounding tissue lesions, left ventricular ejection fraction, ventricular area ratio, pericardial effusion, and examination-related complications were recorded. Bilateral lung lesions were evaluated by using a lung ultrasound score.

RESULTS: The remote ultrasound system successfully and safely performed cardiopulmonary examinations of all patients. Peripheral lung lesions were clearly evaluated. Severe cases of COVID-19 had significantly more diseased regions (median [interquartile range], 6.0 [2.0-11.0] vs 1.0 [0.0-2.8]) and higher lung ultrasound scores (12.0 [4.0-24.0] vs 2.0 [0.0-4.0]) than nonsevere cases of COVID-19 (both, $P < .05$). One nonsevere case (8.3%; 95% CI, 1.5-35.4) and three severe cases (27.3%; 95% CI, 9.7-56.6) were complicated by pleural effusions. Four severe cases (36.4%; 95% CI, 15.2-64.6) were complicated by pericardial effusions (vs 0% of nonsevere cases, $P < .05$). No patients had significant examination-related complications.

INTERPRETATION: Use of the 5G-based robot-assisted remote ultrasound system is feasible and effectively obtains ultrasound characteristics for cardiopulmonary assessment of patients with COVID-19. By following established protocols and considering medical history, clinical manifestations, and laboratory markers, this system might help to evaluate the severity of COVID-19 remotely.

CHEST 2021; 159(1):270-281

KEY WORDS: COVID-19; lung diseases; robotics; telemedicine; ultrasound

ABBREVIATIONS: COVID-19 = coronavirus disease 2019; HRCT = high-resolution CT; LUS = lung ultrasound score; LVEF = left ventricular ejection fraction; RVEDA/LVEDA = right ventricular end-diastolic area/left ventricular end-diastolic area; SARS-CoV-2 = severe acute respiratory syndrome coronavirus 2

AFFILIATIONS: From the Department of Ultrasound Medicine (Drs Ye, Wang, S. Chen, Cui, and Peng), Zhejiang Provincial People's Hospital & People's Hospital of Hangzhou Medical College, Hangzhou, Zhejiang, China; Emergency Center (Drs Zhou and Zhao),

Coronavirus disease 2019 (COVID-19) is mainly transmitted through droplets and in-person contact, and has rapidly spread worldwide.[1,2] As of April 25, 2020, more than 2,700,000 confirmed cases and nearly 190,000 COVID-19-related deaths have been reported. Viral nucleic acid testing verifies infection of severe acute respiratory syndrome coronavirus 2 (SARS-CoV-2), with varying sensitivities (37%-71%) due to differences in specimen type, site and time of collection, and disease course and severity.[3-6] High-resolution CT (HRCT) imaging has been widely used for diagnosis of COVID-19 because of its high spatial resolution. However, it is potentially harmful because the patient is exposed to ionizing radiation, transporting severe cases is risky, and disinfection of the scanner is cumbersome.[7,8] The international consensus on diagnosis and differential diagnosis of lung diseases indicates that bedside ultrasound is an important method of examining and evaluating patients with severe acute illnesses due to the simplicity of the technique and the absence of ionizing radiation.[9,10] Bedside ultrasound has been proposed as a potential diagnostic tool for COVID-19, based on the disease predilection for subpleural regions. However, bedside ultrasound has not been widely implemented because it requires close proximity between the sonographer and the patient, increasing infection risk.[11,12]

Over the past 20 years, advances in computer networks, multimedia, and communication technologies have led to the development of remote ultrasonic robot technology for clinical applications, and a wealth of experience has been accumulated in abdominal, cardiac, pelvic, obstetric, vascular, and thyroid examinations.[13-21] The lack of contact requirement and continuous improvements in safety performance have led to its application for examination of patients with COVID-19 in isolation wards, as it can help to protect examiners against viral infection. In the current study, a 5G-based robot-assisted remote-operated ultrasound system was used for remote examination of patients with COVID-19. We assessed the feasibility of this approach, established an examination and evaluation protocol, and summarized ultrasound characteristics to expand the application of this technology in diagnostics.

Patients and Methods

Patients

The study adhered to the tenets of the Declaration of Helsinki, was approved by the institutional review board of Zhongnan Hospital of Wuhan University, and was performed with the informed consent of the patients or their families. We retrospectively analyzed a total of 23 patients diagnosed with COVID-19 by using nucleic acid testing between March 6, 2020, and April 1, 2020, who were hospitalized in Zhongnan Hospital and were examined by using the 5G-based robot-assisted remote ultrasound system. All patients were classified based on the clinical stage determined by the Guidelines for the Diagnosis and Treatment of Novel Coronavirus Pneumonia (Trial Version 7) prior to the start of the study.[22] The first was the nonsevere group, who satisfied the diagnostic criteria of fever, respiratory tract symptoms, and imaging manifestations of pneumonia. The second was the severe group, who satisfied any one of the following diagnostic criteria: (1) shortness of breath, respiratory rate $\geq$ 30 beats/min; (2) finger oxygen saturation $\leq$ 93% in resting state; (3) pulmonary imaging showing that lesions progressed by $>$ 50% within 24 to 48 h; and (4) $Pao_2/Fio_2 \leq$ 300 mm Hg (1 mm Hg = 0.133 kPa) with Pao_2/Fio_2 corrected according to the following formula for high altitudes ($>$ 1,000 m):

Pao_2/Fio_2 * [atmospheric pressure (mm Hg)/760]

The demographic information and laboratory markers of the 23 patients with COVID-19 were recorded.

Instrument

This study used a robotic ultrasound system, MGIUS-R3 (MGI Tech Co., Ltd.), that integrated robotics, teleoperation, and ultrasound imaging. It could achieve remote robotic control, ultrasound examination, and audio-visual communication. MGIUS-R3 consists of a physician-side subsystem (Fig 1A) and a patient-side subsystem (Fig 1B), which were paired and connected through a 5G network, with a downlink rate of 930 Mbps and an uplink rate of 132 Mbps. The physician-side subsystem comprised the ultrasound display system, audio-visual communication system, and control system, located at Zhejiang Provincial People's Hospital in Hangzhou, Zhejiang Province. A senior sonographer with 15 to 20 years' experience, trained per standardized examination protocol, operated this subsystem. The patient-side subsystem comprised the ultrasound imaging system, audio-visual communication system, and a robotic arm with six

Hubei Clinical Research Center for Emergency and Resuscitation, Zhongnan Hospital of Wuhan University, Wuhan, Hubei, China; Medical aiding team for COVID-19 in Hubei (Drs Shao, Hong, Huang, and L. Chen), Zhejiang Provincial People's Hospital, Hangzhou, Zhejiang, China; MGI Tech Co., Ltd. (Dr Xiong), Shenzhen, Guangdong, China; and Gennlife (Beijing) Biotechnology Co. Ltd. (Dr Tong), Haidian, Beijing, China.

Drs Ye and Zhou contributed equally to the article and should be considered co-first authors.

FUNDING/SUPPORT: This study was supported by the Emergency Response Project of Hubei Science and Technology Department [2020FCA023 to Y. Z.].

CORRESPONDENCE TO: Legao Chen, MD, Medical aiding team for COVID-19 in Hubei, Zhejiang Provincial People's Hospital, 158 Shangtang Rd, Hangzhou, Zhejiang, 310014, China; e-mail: chenlegao@126.com

DOI: https://doi.org/10.1016/j.chest.2020.06.068

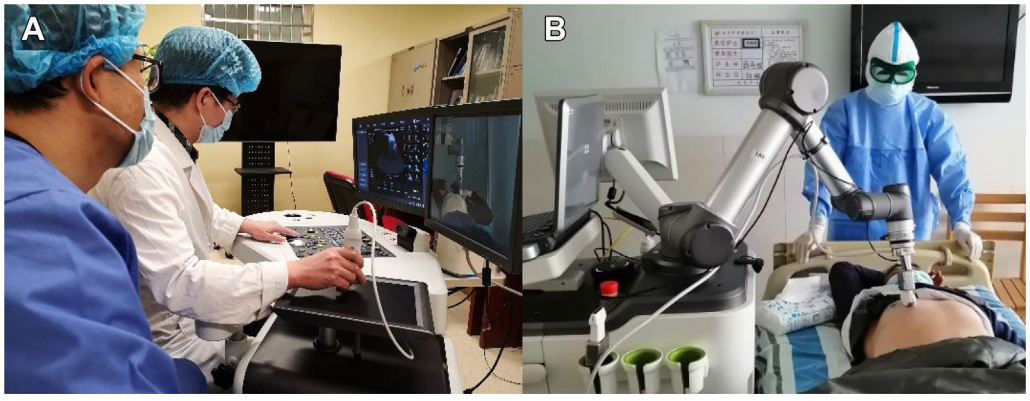

Figure 1 – *A, The sonographer on the physician-side manipulates a simulated probe, and the control signal is captured through the ultrasound control panel and sent to the patient-side following the control protocol, with all movements replicated by the remote robotic arm in real-time. The probe has three degrees of freedom for rotation, with the position sensor having two degrees of freedom for movement in the horizontal plane. The "UP" button and pressure sensor have one degree of freedom each for up and down movements. B, The robotic arm and a force sensor on the patient-side are used to execute the motion instructions from the physician-side and to complete the examinations. The ultrasound imaging results are captured and transferred to the physician-side through the Internet. The audio-visual communication system allows communication between the sonographer and the patient.*

degrees-of-freedom, which was located next to the patient's bed in the isolation ward of Zhongnan Hospital of Wuhan University, Hubei Province. The ultrasound imaging system was manufactured by Wisonic Medical Technology Co., Ltd., and had a 1.0 to 5.5 MHz convex array probe, which was equipped on the robotic arm.

The MGIUS-R3 had multiple protection measures to ensure patient safety: (1) the start reminder was prompted simultaneously on both terminals when the robotic arm started; (2) an emergency stop button was installed next to the ultrasound probe socket of the robotic arm on the patient-side; and (3) the robotic arm had speed ($\leq$ 0.675 m/s for the convex array probe and $\leq$ 0.275 m/s for the linear array probe) and pressure (3-20 N) limit settings, with parameter changes taking effect synchronously (the robotic arm stopped moving once the set value exceeded the standard).

Medical alcohol (75% concentration) kills SARS-CoV-2 and evaporates quickly, and was thus used to disinfect the patient-side instrument surface. It was the first choice in disinfectant, although it would damage the machine. The surface residues were then removed with disinfectant paper. The probe was disinfected once per patient. If it contacted mucous membranes or wounds, a medical ultrasonic coupling agent with a disinfection function or special disinfectant was used. Finally, the instrument was disinfected regularity with UV light once daily for 1 h each time.

Examination Protocol

The robot-assisted remote ultrasound examination was performed for patients with COVID-19 as follows. First, the clinician initiated a consultation request through the remote system after a comprehensive evaluation of patients with COVID-19 in the isolated wards. The patient information was registered in the system at the same time.

Second, the remote consultation expert switched on the physician-side subsystem and ensured 5G network connection and patient-side subsystem recognition. Through the audio-visual communication system, the expert guided the patient to adopt the appropriate examination posture. The expert then started the robotic arm, performed the examination of the lungs and hearts of the patient with COVID-19, and saved the ultrasound images or videos. The probe scanned vertically along the intercostal space in the following order: inside to outside, top to bottom, and front to back. Each lung was divided into upper and lower parts, totaling 12 zones, using the parasternal, front axillary, posterior axillary, and paraspinal lines as boundaries.[23,24] The 12 zones were marked as R or L, for right or left, respectively, with corresponding numbers, for easy recording and data analysis (Fig 2). Multipoint examination was performed for each zone. Cardiac ultrasound evaluation was simultaneously performed by using the left ventricular short-axis view.

Finally, patient data (eg, patient characteristics, medical history, clinical manifestations, laboratory markers) were presented after completion of

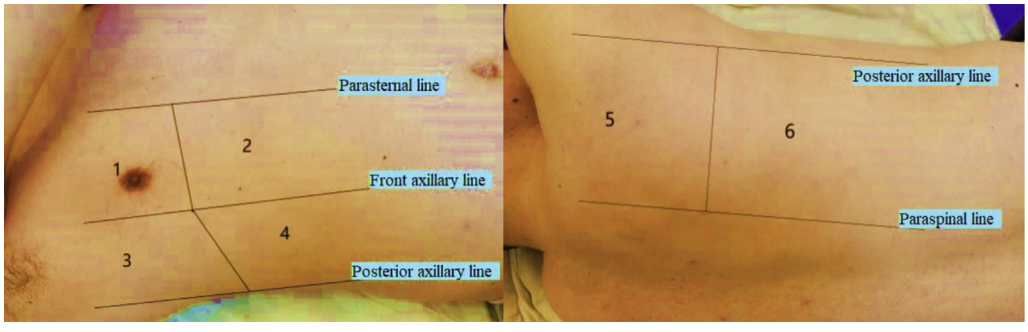

Figure 2 – *Twelve zones were marked as R or L, for right or left, respectively, plus a corresponding number. For example, the right upper front zone, right lower front zone, right upper side zone, right lower side zone, right upper rear zone, and right lower rear zone were sequentially marked as R1 to R6; similar notation was used on the left.*

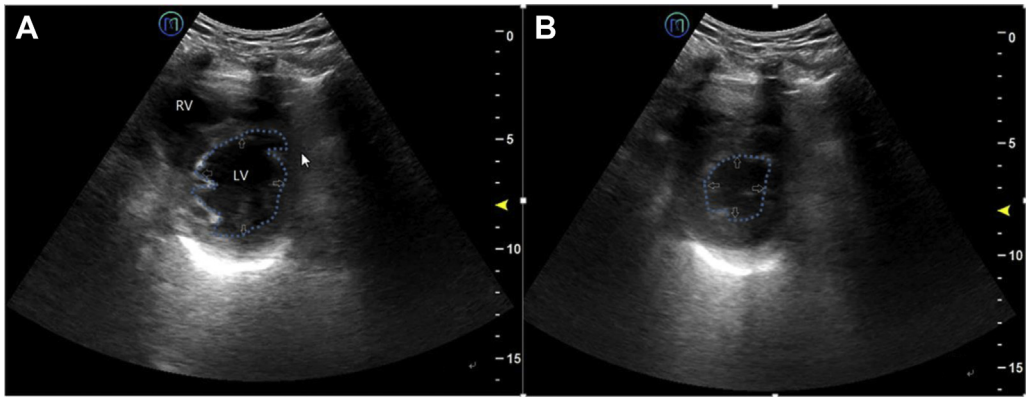

Figure 3 – *Left ventricular ejection fraction for evaluation of left ventricular contractile function, using the "eyeballing" method, on the short-axis view of the LV. The main observation indicators include endocardial movement, end-systolic left ventricular cavity size, and myocardial thickness changes. The outer edge of the LV is visible (white arrow). A, End-diastolic left ventricular cavity size (blue dotted line). B, End-systolic left ventricular cavity size (blue dotted line). LV = left ventricle; RV = right ventricle.*

the examination. After storing and analyzing the examination results, the expert issued a diagnostic report to the attending clinicians to guide further treatment.

An assistant was needed during the examination, who aided in disinfecting the instrument, guiding patients to conduct examinations in an orderly manner, applying medical coupling

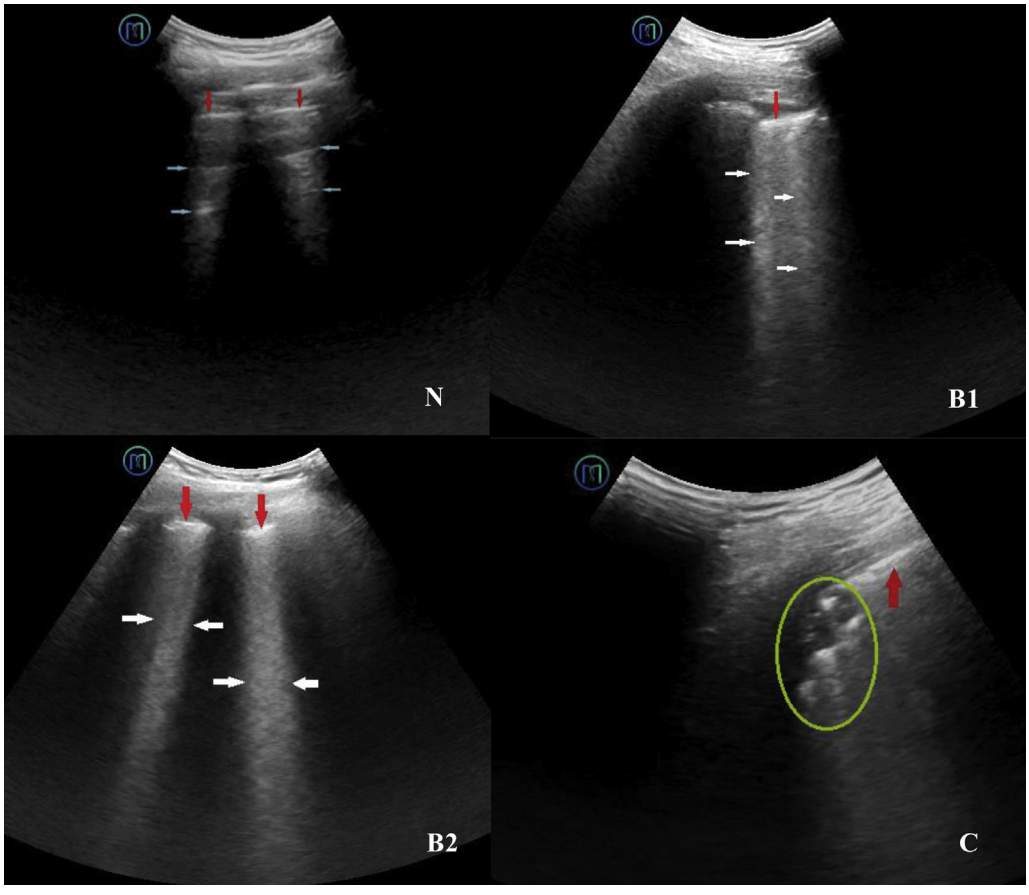

Figure 4 – *N is characterized by the presence of lung sliding and A lines (blue arrows), or less than three B lines. The pleural line is continuous and regular (red arrows) and has a score of zero. B1 is characterized by multiple regularly or irregularly distributed B lines (white arrows) that originate from the pleural line. The pleural line is thick and rough (red arrows) and has a score of one. B2 is characterized by several intercostal spaces fully occupied by the coalescent B lines (white arrows). The pleural line is thick and rough (red arrows) and has a score of two. C is characterized by tissue echogenicity (green circle), known as pulmonary consolidation. The pleural line is broken (red arrows) and has a score of three.*

agents, and appropriately adjusting the position of severely ill patients.

Image Acquisition and Analysis

The acquired ultrasound images included the following information[25,26]: (1) lesion pattern, including the disappearance of lung sliding, B-line increase, and lung consolidation; (2) distribution characteristics, including the number, location, edge, and depth; (3) other findings such as adjacent pleural thickening or continuity interruption, and the presence or absence of pericardial effusion and pleural effusion; and (4) quantitative information such as maximum depth of pericardial and pleural effusions, left ventricular ejection fraction (LVEF; standard value, 50%-70%) (Fig 3) and the ratio of right ventricular end-diastolic area to left ventricular end-diastolic area (RVEDA/LVEDA) (endocardium-tracing method, on the left ventricular short-axis view; standard value < 0.6). The storage duration of dynamic images was 3 to 5 s.

Lung ultrasound characteristics were classified into four categories (N, B1, B2, and C), and scored as 0 to 3 points (Fig 4).[27-30] The worst ultrasound characteristic was considered representative of a particular lung zone and given the corresponding score.[31,32] Scores of the 12 examined zones were summed to calculate the lung ultrasound score (LUS), ranging from 0 to 36. LUS videos were analyzed offline by two sonographers, who were blinded to the clinical data and each other's ultrasound diagnoses.

Statistical Analysis

Statistical analyses were performed by using IBM SPSS software version 23 (IBM SPSS Statistics, IBM Corporation). Continuous variables are presented as mean ± SD (normal distribution) or median and interquartile range (non-normal distribution). Categorical variables are presented as percentages of the total. Prevalence data are reported using the 95% CI. Comparisons between groups were made by using either parametric Student *t* tests or nonparametric Mann-Whitney *U* tests. The statistical significance of differences among categorical variables was determined by using the χ^2 test or Fisher exact test. *P* values < .05 were defined as statistically significant.

Results

Patient Information

Of the 23 patients, 12 were nonsevere cases of COVID-19 (four male subjects and eight female subjects) with a mean ± SD age of 53.5 ± 13.5 years, and 11 were severe cases (eight male subjects and three female subjects) with a mean age of 67.2 ± 15.9 years (Table 1). There were 40 different comorbidities. Mean oxygen saturation was lower in severe cases than in nonsevere cases (mean, 93.0 ± 2.1% vs 99.8 ± 0.6%; $P < .05$).

On admission, all patients had a WBC count in the normal range. Neutrophils were mostly in the normal range. Almost one-half of the severe patients had a below-normal eosinophil count, and more than one-half of them had a below-normal lymphocyte count. A few patients with nonsevere disease and more than one-half of patients with severe disease had cardiac markers exceeding the normal range. One-quarter of nonsevere patients and all severe patients had C-reactive protein levels above the normal range. Almost one-half of the nonsevere cases and almost three-quarters of the severe cases had an erythrocyte sedimentation rate above normal. Few patients in both groups had excessive procalcitonin levels. One-quarter of the nonsevere group and almost three-quarters of the severe group had excessive cytokine levels (Table 1).

Differences in age, oxygen saturation, eosinophils, lymphocytes, cardiac markers, C-reactive protein, and cytokines between the groups were statistically significant ($P < .05$) (Table 1).

Feasibility and Safety

A standard examination protocol was established (Fig 5). According to the protocol, a cardiopulmonary assessment was completed successfully for all patients by using the 5G-based robot-assisted remote ultrasound system. Each examination took 10 to 20 min, on average, and there was no noticeable delay in scanning. We obtained ultrasound image information, such as distribution characteristics, morphology of the lungs and surrounding tissue lesions, LVEF, RVEDA/LVEDA, pericardial and pleural effusion, and LUS. No patient had significant examination-related complications.

Ultrasound Characteristics

Peripheral lung lesions could be evaluated clearly and effectively using ultrasonography (Table 2). The severe cases had significantly more diseased regions (including B1, B2, or C) (6.0 [2.0-11.0] vs 1.0 [0.0-2.8]) and a higher LUS (12.0 [4.0-24.0] vs 2.0 [0.0-4.0]) than nonsevere cases (both, $P < .05$). Lesions tended to be distributed in the lower lobes. There were 13 dorsal lung lesion regions (9% [13 of 144]; 95% CI, 5.4-14.8) in the nonsevere group and 36 in the severe group (27.3% [36 of 132]; 95% CI, 20.4-35.4). The incidence of lung consolidation was 2.8% (4 of 144; 95% CI, 1.1-6.9) in the nonsevere group (maximum length, 20 mm; depth, 5 mm) and 15.2% (20 of 132; 95% CI, 10.0-22.2) in the severe group, with a wide range of lengths and depths. One nonsevere case (8.3%; 95% CI, 1.5–35.4) and three severe cases (27.3%; 95% CI, 9.7-56.6) had pleural effusions (5- and 14-mm deep, respectively), and the pleural line was thick and rough (Fig 6).

TABLE 1] Clinical Characteristics and Laboratory Results (N = 23)

Patient Information	Group		*P* Value
	Nonsevere Type (n = 12)	Severe Type (n = 11)	
Clinical characteristics			
Age, y			.004[a]
Mean ± SD	53.5 ± 13.5	67.2 ± 15.9	
Range	34-71	35-81	
Sex			.100
Male	4	8	
Female	8	3	
Oxygen saturation, %	99.8 ± 0.6	93.0 ± 2.1	< .001[a]
Comorbidities			
Hyperlipidemia	6 (50%)	1 (9.1%)	.069
Hypertension	5 (41.7%)	6 (54.5%)	.684
Diabetes	2 (16.7%)	1 (9.1%)	.227
TB	0 (0%)	2 (18%)	.217
COPD	0 (0%)	2 (18%)	.217
Bacterial infections of the lung	1 (8.3%)	4 (36.4%)	.155
Varicose veins of the lower extremities	2 (16.7%)	4 (36.4%)	.371
Cerebral hemorrhage	0 (0%)	1 (9.1%)	.478
Chronic kidney disease	1 (8.3%)	2 (18.2%)	.590
Laboratory results			
WBC count			
Normal	12 (100%)	11 (100%)	
Increased	0 (0%)	0 (0%)	
Decreased	0 (0%)	0 (0%)	
Neutrophil count			
Normal	12 (100%)	10 (90.9%)	
Increased	0 (0%)	1 (9.1%)	.478
Decreased	0 (0%)	0 (0%)	
Eosinophil count			
Normal	12 (100%)	6 (54.5%)	
Increased	0 (0%)	0 (0%)	
Decreased	0 (0%)	5 (45.5%)	.014[a]
Lymphocyte count			
Normal	12 (100%)	4 (36.4%)	
Increased	0 (0%)	0 (0%)	
Decreased	0 (0%)	7 (63.6%)	.001[a]
Cardiac markers			
Normal	10 (83.3%)	4 (36.4%)	
Increased	2 (16.7%)	7 (63.6%)	.036[a]
Decreased	0 (0%)	0 (0%)	
C-reactive protein			
Normal	9 (75%)	0 (0%)	
Increased	3 (25%)	11 (100%)	< .001[a]
Decreased	0 (0%)	0 (0%)	

(Continued)

TABLE 1] *(Continued)*

Patient Information	Group		*P* Value
	Nonsevere Type (n = 12)	Severe Type (n = 11)	
Erythrocyte sedimentation rate			
Normal	7 (58.3%)	3 (27.7%)	
Increased	5 (41.7%)	8 (72.3%)	.214
Decreased	0 (0%)	0 (0%)	
Procalcitonin			
Normal	10 (83.3%)	9 (81.8%)	
Increased	2 (16.7%)	2 (18.2%)	.134
Decreased	0 (0%)	0 (0%)	
Cytokine			
Normal	9 (75%)	3 (27.7%)	
Increased	3 (25%)	8 (72.3%)	.039[a]
Decreased	0 (0%)	0 (0%)	

Data are presented as No. (%) of patients or mean ± SD unless otherwise indicated. Cardiac markers include aspartate aminotransferase, creatine kinase (CK), CK-myocardial band, α-hydroxybutyrate dehydrogenase, lactate dehydrogenase, high-sensitivity troponin I, and N-terminal pro–B-type natriuretic peptide. An increase in any indicator indicates the abnormality of the cardiac marker. Cytokine includes interferon-γ, IL-2, IL-4, IL-6, and IL-10. An increase in any indicator indicates abnormality of the cytokine. Normal range of laboratory indicators: WBC, 3.5 to 9.5 × 10^9/L; neutrophils, 1.8 to 6.3 × 10^9/L; eosinophils, 0.02 to 0.52 × 10^9/L; lymphocytes, 1.1 to 3.2 × 10^9/L. Cardiac injury markers: aspartate aminotransferase, 13 to 35 U/L; CK, < 140 U/L; CK- myocardial band, 0 to 25 U/L; α-hydroxybutyrate dehydrogenase, 74 to 199 U/L; lactate dehydrogenase, 125 to 243 U/L; myoglobin, < 140.1 ng/mL; high-sensitivity troponin I, 0 to 26.2 pg/mL; N-terminal pro–B-type natriuretic peptide, 0 to 900 pg/mL; erythrocyte sedimentation rate, 0 to 15 mm/h; C-reactive protein, 0 to 3 mg/L; platelet count, < 0.05 ng/mL. Cytokine: interferon-γ, 0.1 to 18 pg/mL; IL-2, 0.1 to 4.1 pg/mL; IL-4, 0.1 to 3.2 pg/mL; IL-6, 0.1 to 2.9 pg/mL; IL-10, 0.1 to 5.0 pg/mL.
[a]*P* < .05.

The LVEF and ventricular area ratio of the heart were normal in all 23 cases. Four severe cases (36.4%; 95% CI, 15.2-64.6) were complicated by pericardial effusions 3 to 10 mm wide (vs 0% of the nonsevere cases; $P < .05$) (Fig 7).

Discussion

Cardiopulmonary assessment was successfully and safely completed in all patients with COVID-19 using the 5G-based robot-assisted remote ultrasound system. Image

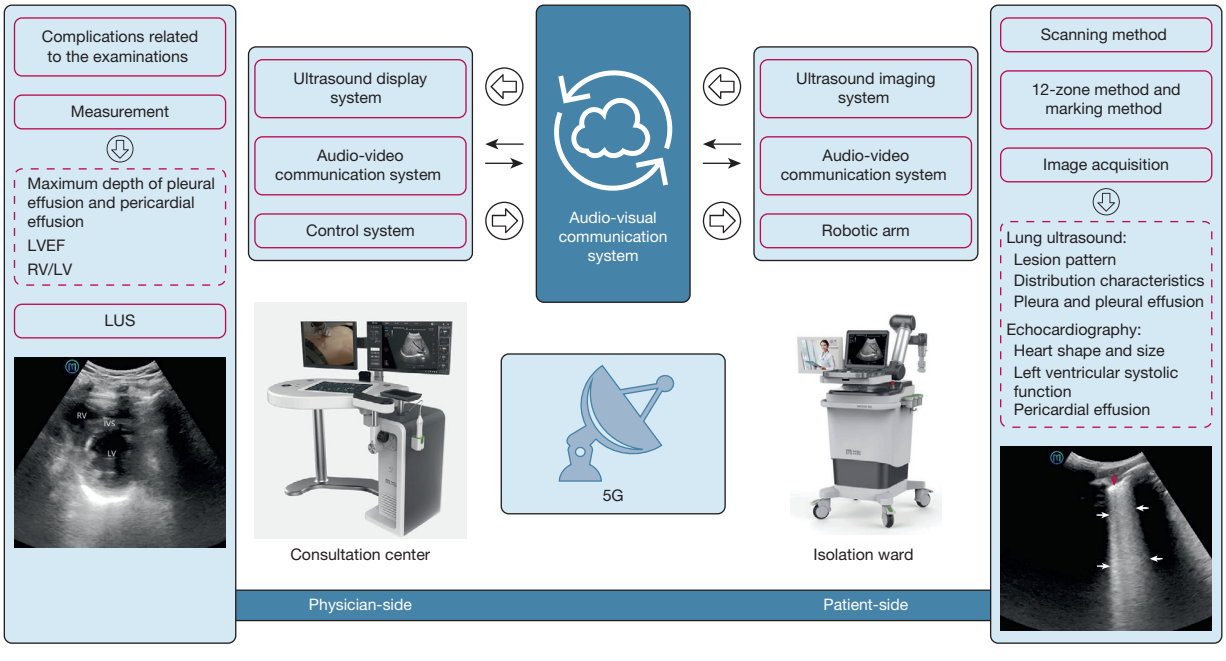

Figure 5 – *Examination and evaluation protocol of the 5G-based robot-assisted remote ultrasound system. IVS = intraventricular septum; LUS = lung ultrasound score; LVEF = left ventricular ejection fraction. See Figure 3 legend for expansion of other abbreviations.*

TABLE 2] Ultrasound Results in Patients With Coronavirus Disease 2019 (N = 23)

Group	No.	Echocardiography		Lung Ultrasound		
		LVEF (%)	Pericardial Effusion	Diseased Regions (B1 + B2 + C)	Lung Ultrasound Score	Pleural Effusion
Nonsevere	12	64.2 ± 2.9	0	1.0 (0.0-2.8)	2.0 (0.0-4.0)	1 (8.3)
Severe	11	63.6 ± 2.3	4 (36.4)	6.0 (2.0-11.0)	12.0 (4.0-24.0)	3 (27.3)
P value		.635	.037[a]	.004[a]	.004[a]	.317

Data are presented as mean ± SD, median (interquartile range), and No. (%). LVEF = left ventricular ejection fraction.
[a]$P < .05$.

acquisition, labeling, and analysis were performed as per the established examination protocol, without complications. This underscores that the advances and safety of current computer networks and communication technology allows long-distance ultrasonic image acquisition, transmission, analysis, and processing, with high-precision synchronization of multiple audio-visual signals. It can assist in the construction of remote real-time ultrasound collaborations, interactive operability, and consultation modes. Current ultrasonic robot technology has made considerable advances, and rich experience has been accumulated through many clinical applications.[13-21,33] Studies have indicated that the quality of images captured by robot-assisted remote ultrasound systems correlate well with those captured by conventional ultrasound.[34-36]

Robot technology has been reported for assistance in the diagnosis and treatment of lung diseases previously,[37-39] but the application of a 5G-based robot-assisted remote ultrasound system for use in lung disorders has not been reported to date. 5G networks have a high data transmission rate (peak rate up to 20 Gbps) and low network delay (approximately 1-10 ms). Consequently, no noticeable delay occurred during scanning, and each examination was completed quickly, facilitating further clinical implementation of the 5G-based robot-assisted remote ultrasound system.[40] In addition, we used strict infection control practices, including the hand hygiene of assistants and cleaning and disinfection of the floor, object surfaces, and the patient-side instrument. In summary, the application of this system allowed us to surpass time and space restrictions and guaranteed minimization of cross-infection risk in the assessment of patients with COVID-19.

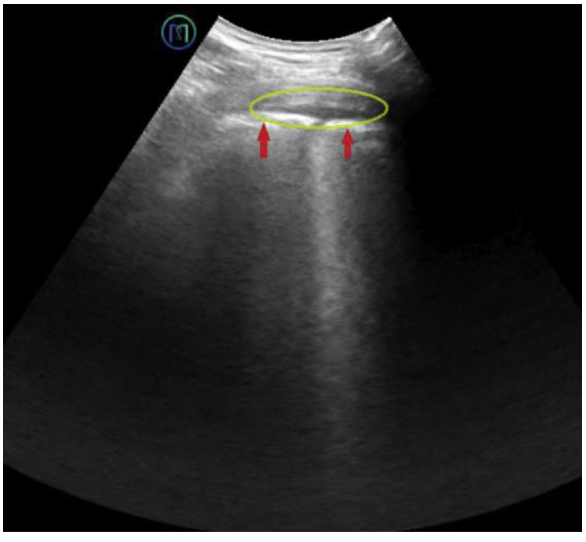

Figure 6 – *Pleural effusion is characterized by an echoless dark area (green circle) in the pleural cavity. The pleural line is thick and rough (red arrows).*

HRCT imaging is widely used for COVID-19 diagnosis, offering advantages of high spatial resolution and multiplanar and multidirectional display of lesion details, although it also has unavoidable disadvantages such as the potential harm of ionizing radiations and the risk of transporting critically ill patients. Based on HRCT imaging, lung lesions are mainly distributed under the pleura of the outer one-third of the lung field, particularly in the dorsal and bottom lung regions. For patients with advanced stage and severe COVID-19, CT shows diffuse lung lesions, with extensive exudation and lung consolidation mainly in the lower lobe, along with pleural effusion.[41,42] The accumulated CT diagnostic experience and lesion distribution characteristics provided a theoretical and technical reference for the application of lung ultrasound in COVID-19.[43]

Ultrasonography has advantages of convenience and dynamics.[44] It facilitates the diagnosis of lung diseases, rapid confirmation of acute respiratory failure causes, shock classification, qualitative assessment of pleural effusion (free or wrapped), and dynamic monitoring of diaphragm activity to predict offline extubation success.[9-10] Studies have shown that patients with COVID-19 have characteristic lung ultrasound manifestations, such as coalescent B lines and subpleural

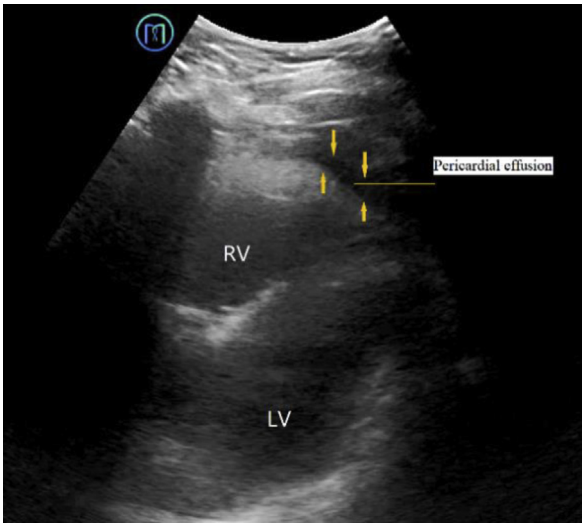

Figure 7 – *Pericardial effusion is characterized by an echoless dark area (orange arrows) in the pericardial cavity. See Figure 3 legend for expansion of abbreviations.*

lung consolidation, mostly in the posterior and lower parts of the lung.[12]

In addition, the rapid development of remote ultrasonic and 5G communication technology has improved the feasibility of using a 5G-based robot-assisted remote ultrasound system in COVID-19 diagnosis. In this retrospective ultrasound study, B lines, lung consolidation, or atelectasis was mainly distributed in the lung periphery and significantly in the dorsal lung region, consistent with reported CT results.[45] The number of diseased lung regions, incidence and number of B lines, and incidence of lung consolidation were significantly higher in the severe group than in the nonsevere group. Ultrasound found no abnormalities in the lungs of four nonsevere cases. One nonsevere case and three severe cases had pleural effusion. Thus, ultrasonography might be helpful for evaluating COVID-19 severity, and the 5G-based robot-assisted remote ultrasound system could achieve the same effect as a face-to-face, close-range ultrasound examination.

The LUS was used for overall lung evaluation of patients with COVID-19 in our study. The LUS was significantly higher in the severe group than in the nonsevere group, probably because vascular and inflammatory reactions were more exaggerated in severe cases, causing some bronchial embolisms to block the bronchiole and terminal bronchiole partially or completely, triggering lung atelectasis or consolidation, eventually leading to ventilation dysfunction.[46-50] Current literature[29] indicates that, in a controlled human model of lung air content variation, the LUS can reliably record lung aeration changes. This method was successfully applied to assess extravascular lung water, which predicts failure of mechanical ventilation weaning and allows monitoring aeration in patients undergoing extracorporeal membrane oxygenation. The LUS is closely related to several ARDS diagnostic and prognostic indexes such as the extravascular lung water index, lung injury score, respiratory system compliance, and Pao_2/Fio_2, and it serves as a death-risk prediction index.[41,42,51] In this study, one nonsevere case (1 of 12 [8.3%]) and four severe cases (4 of 11 [36.4%]) also had pulmonary bacterial infections, with an LUS of 14 and 4 to 29, respectively. Compared with patients with COVID-19 with nonpulmonary bacterial infections, these patients might have displayed aggravated lung lesions, but this topic requires further research. Some studies[51] have shown that patients with COVID-19 with comorbidities have significantly higher risks of ICU admission, invasive ventilation, and death than patients without comorbidities, with risk increasing proportionately to the number of comorbidities.

The 5G-based robot-assisted remote ultrasound system was also used for cardiac examination in this study, although it was limited by the patient's position, probe selection (only a 1.0-5.5 MHz convex array probe), and the robotic arm's operating angle. The left ventricular short-axis view offered the only clear view that could be used to assess the size and function of the ventricle. We measured the areas of the right and left ventricles at end-diastole and calculated the area ratio (RVEDA/LVEDA). When the ratio is > 0.6, it indicates that the right ventricle is dilated (ie, potential impaired function). When accompanied by contradictory interventricular septal movements, this finding indicates pulmonary heart disease. Moreover, we used the "eyeballing" visual estimation method to quickly assess the LVEF and left ventricular wall motion. Studies have shown that this method has a good correlation with radionuclide scanning and other quantitative methods. Because this method is readily and quickly performed, it could be used in routine echocardiography. The examination results could help to rule out lung diseases caused by cardiogenic factors (eg, cardiogenic pulmonary edema), clarify the cause and classification of shock, and assess fluid responsiveness.[52-54] Some patients with COVID-19 have obvious cardiac dysfunction, but all the study patients had normal RVEDA/LVEDA and LVEF, perhaps due to the limited viral damage to myocardial cells or damage control by early treatment.[45,46,55] Four

patients with severe COVID-19 (4 of 11 [36.4%]) had pericardial effusions (3-10 mm wide), and one of these had increased α-hydroxybutyrate dehydrogenase (291 U/L) and lactic acid dehydrogenase (375 U/L) levels. There were no such cases in the nonsevere group; thus, the underlying mechanism requires investigation.

Thus, the 5G-based robot-assisted remote ultrasound system offers a feasible option for cardiopulmonary evaluation of patients with COVID-19. The establishment of an examination protocol helped in performing standardized examinations, as well as in the learning, training, and promotion of the technology. However, the study had some limitations. Because we conducted ultrasound examination for patients with COVID-19 only at a specific disease stage, dynamic evaluation of disease progression was not possible. Hence, further follow-up ultrasound data must be collected, and their correlations with clinical findings should be analyzed to observe the evolution and outcome of the disease. Lung diseases of different etiologies can have similar ultrasound characteristics; consequently, this method cannot be used to determine etiology. Differences between the two groups in age, oxygen saturation, eosinophils, lymphocytes, cardiac markers, C-reactive protein, and cytokines were statistically significant ($P < .05$). Therefore, a comprehensive assessment needs to be conducted in conjunction with the medical history, clinical manifestation, and laboratory test data.

In addition, the 5G-based robot-assisted remote ultrasound system is still in its infancy and requires further improvements. For example, restrictions of the examination position of the patient (especially critically ill patients) and operating angle of the robotic arm made some body parts difficult for the robotic arm to reach. The use of only one convex array probe markedly affects the quality of cardiac images due to the frequency limitation. It would also be valuable to include control (non-COVID-19) patients in a later study or to assess comparability between telerobotic and conventional ultrasound for verifying diagnostic accuracy of cardiopulmonary examinations. In addition, this analysis was a single-center study with a small sample size. More sample data could be obtained through multicenter cooperation in the future to verify the value of the 5G-based robot-assisted remote ultrasound system in lung disease assessment. Finally, the impact of the limitations of lung ultrasound on the examination results should be considered. The restrictions included operator dependence, patient dependence (eg, examination posture, subcutaneous emphysema, chest wall dressing interference), and lesion location dependence (eg, in the center of the lung).

Although the initial application of the 5G-based robot-assisted remote ultrasound system in the COVID-19 epidemic has achieved good results, it cannot wholly replace CT imaging and other examinations. With the in-depth application of artificial intelligence in the medical field, integrating artificial intelligence into robot-assisted remote ultrasound systems would greatly increase the scope of use for this technology, facilitate the diagnosis of lung lesions objectively and accurately, and implement automatic switching between probes on the ultrasonic robot system to facilitate optimal imaging of multiple organs and improve image quality.[56-58]

Interpretation

This study showed that the 5G-based robot-assisted remote ultrasound system is a feasible option for safely and effectively performing cardiopulmonary examinations of patients with COVID-19 in isolation wards.

Acknowledgments

Author contributions: L. C. is the guarantor of the paper. L. C., Y. Z., C. P., R. Y., and X. Z. undertook study design. F. S., J. W., W. T., J. H., and H. H. enrolled patients and acquired data. F. S., S. C., A. C., W. T., J. H., H. H., and L. X. undertook statistical analysis. R. Y., X. Z., A. C., J. W., L. C., Y. Z., C. P., and L. X. drafted the manuscript and revised it critically. All authors reviewed the manuscript and approved the final version.

Financial/nonfinancial disclosures: None declared.

Role of sponsors: The sponsor had no role in the design of the study, the collection and analysis of the data, or the preparation of the manuscript.

Other contributions: The authors express their appreciation for all of the emergency services, nurses, doctors, and other hospital staff for their efforts to respond to the COVID-19 outbreak.

References

1. Xu X, Chen P, Wang J, et al. Evolution of the novel coronavirus from the ongoing Wuhan outbreak and modeling of its spike protein for risk of human transmission. *Sci China Life Sci*. 2020;63(3):457-460.
2. Phan LT, Nguyen TV, Luong QC, et al. Importation and human-to-human transmission of a novel coronavirus in Vietnam. *N Engl J Med*. 2020;382(8):872-874.
3. Li Z, Yi Y, Luo X, et al. Development and clinical application of a rapid IgM-IgG combined antibody test for SARS-CoV-2 infection diagnosis. *J Med Virol*. In press. https://doi.org/10.1002/jmv.25727.
4. Wang L, Yang S, Yan X, et al. Comparing the yield of oropharyngeal swabs and sputum for detection of 11 common pathogens in hospitalized children with lower respiratory tract infection. *Virol J*. 2019;16(1):84.
5. Ai T, Yang Z, Hou H, et al. Correlation of chest CT and RT-PCR testing in coronavirus disease 2019 (COVID-19) in China: a report of 1014 cases. *Radiology*. 2020;296(2):E32-E40.
6. Li Y, Yao L, Li J, et al. Stability issues of RT-PCR testing of SARS-CoV-2 for hospitalized patients clinically diagnosed with COVID-19. *J Med Virol*. 2020;92(7):903-908.
7. Zakhari R, Sterrett SE. Attitudes toward evidence-based clinical decision support tools to reduce exposure to ionizing radiation: the Canadian CT Head Rule. *J Am Assoc Nurse Pract*. 2016;28(12):659-667.
8. Jeffrey MA. Radiation risk from CT: implications for cancer screening. *AJR Am J Roentgenol*. 2013;201(1):W81-W87.
9. Liu J, Copetti R, Sorantin E, et al. Protocol and guidelines for point-of-care lung ultrasound in diagnosing neonatal pulmonary diseases based on international expert consensus. *J Vis Exp*. 2019;145.
10. Song G, Bae SC, Lee YH. Diagnostic accuracy of lung ultrasound for interstitial lung disease in patients with connective tissue diseases: a meta-analysis. *Clin Exp Rheumatol*. 2016;34(1):11-16.
11. Rubin GD, Ryerson CJ, Haramati LB, et al. The role of chest imaging in patient management during the COVID-19 pandemic: a multinational consensus statement from the Fleischner Society. *Radiology*.2020;296(1):172-180.
12. Soldati G, Smargiassi A, Inchingolo R, et al. Is there a role for lung ultrasound during the COVID-19 pandemic? *J Ultrasound Med*. 2020;39(7):1459-1462.
13. Fincke EM, Padalka G, Lee D, et al. Evaluation of shoulder integrity in space: first report of musculoskeletal US on the International Space Station. *Radiology*. 2005;234(2):319-322.
14. Delgorge C, Courrèges F, Al Bassit L, et al. A tele-operated mobile ultrasound scanner using a light-weight robot. *IEEE Trans Inf Technol Biomed*. 2005;9(1):50-58.
15. Adams SJ, Burbridge BE, Badea A, et al. Initial experience using a telerobotic ultrasound system for adult abdominal sonography. *Can Assoc Radiol J*. 2017;68(3):308-314.
16. Avgousti S, Panayides AS, Jossif AP, et al. Cardiac ultrasonography over 4G wireless networks using a tele-operated robot. *Healthc Technol Lett*. 2016;3(3):212-217.
17. Georgescu M, Sacccomandi A, Baudron B, et al. Remote sonography in routine clinical practice between two isolated medical centers and the university hospital using a robotic arm: a 1-year study. *Telemed J E Health*. 2016;22(4):276-281.
18. Arbeille P, Capri A, Ayoub J, et al. Use of a robotic arm to perform remote abdominal telesonography. *AJR Am J Roentgenol*. 2007;188(4):W317-W322.
19. Arbeille P, Ruiz J, Herve P, et al. Fetal tele-echography using a robotic arm and a satellite link. *Ultrasound Obstet Gynecol*. 2005;26(3):221-226.
20. Martinelli T, Bosson JL, Bressollette L, et al. Robot-based tele-echography: clinical evaluation of the TER system in abdominal aortic exploration. *J Ultrasound Med*. 2007;26(11):1611-1616.
21. Boman K, Olofsson M, Berggren P, et al. Robot-assisted remote echocardiographic examination and teleconsultation: a randomized comparison of time to diagnosis with standard of care referral approach. *JACC Cardiovasc Imaging*. 2014;7(8):799-803.
22. Lin L, Li TS. Interpretation of "Guidelines for the Diagnosis and Treatment of Novel Coronavirus (2019-nCoV) Infection by the National Health Commission (Trial Version 5)" [in Chinese]. *Zhonghua Yi Xue Za Zhi*. 2020;100(11):805-807.
23. Volpicelli G, Caramello V, Cardinale L, et al. Bedside ultrasound of the lung for the monitoring of acute decompensated heart failure. *Am J Emerg Med*. 2008;26(5):585-591.
24. Singh Y, Tissot C, Fraga MV, et al. International evidence-based guidelines on point of care ultrasound (POCUS) for critically ill neonates and children issued by the POCUS Working Group of the European Society of Paediatric and Neonatal Intensive Care (ESPNIC). *Crit Care*. 2020;24(1):65.
25. Lichtenstein DA. BLUE-protocol and FALLS-protocol: two applications of lung ultrasound in the critically ill. *Chest*. 2015;147(6):1659-1670.
26. Shahabi J, Zavar R, Amirpour A, et al. Right ventricular (RV) echocardiographic parameters in patients with pulmonary thromboembolism (PTE). *ARYA Atheroscler*. 2018;14(2):78-84.
27. Chavez MA, Shams N, Ellington LE, et al. Lung ultrasound for the diagnosis of pneumonia in adults: a systematic review and meta-analysis. *Respir Res*. 2014;15(1):50.
28. Caltabeloti FP, Rouby JJ. Lung ultrasound: a useful tool in the weaning process? *Rev Bras Ter Intensiva*. 2016;28(1):5-7.
29. Zhao Z, Jiang L, Xi X, et al. Prognostic value of extravascular lung water assessed with lung ultrasound score by chest sonography in patients with acute respiratory distress syndrome. *BMC Pulm Med*. 2015;15:98.
30. Soummer A, Perbet S, Brisson H, et al. Ultrasound assessment of lung aeration loss during a successful weaning trial predicts postextubation distress. *Crit Care Med*. 2012;40(7):2064-2072.
31. Bouhemad B, Brisson H, Le-Guen M, et al. Bedside ultrasound assessment of positive end-expiratory pressure-induced lung recruitment. *Am J Respir Crit Care Med*. 2011;183(3):341-347.
32. Bouhemad B, Liu ZH, Arbelot C, et al. Ultrasound assessment of antibiotic-induced pulmonary reaeration in ventilator-associated pneumonia. *Crit Care Med*. 2010;38(1):84-92.
33. Sengupta PP, Narula N, Modesto K, et al. Feasibility of intercity and trans-Atlantic telerobotic remote ultrasound: assessment facilitated by a nondedicated bandwidth connection. *JACC Cardiovasc Imaging*. 2014;7(8):804-809.
34. Liu Yanhua, Zhang Yuanji, Mei Li, et al. Preliminary application study of using tele-ultrasound robot system in volunteers. *Chinese J Ultrasonography*. 2019;28(1):66-70.
35. Arbeille P, Provost R, Zuj K, et al. Tele-operated echocardiography using a robotic arm and an internet connection. *Ultrasound Med Biol*. 2014;40(10):2521-2529.
36. Adams SJ, Burbridge BE, Badea A, et al. A crossover comparison of standard and telerobotic approaches to prenatal sonography. *J Ultrasound Med*. 2018;37(11):2603-2612.
37. Yang Y, Jiang S, Yang Z, et al. Design and analysis of a tendon-based computed

tomography-compatible robot with remote center of motion for lung biopsy. *Proc Inst Mech Eng H*. 2017;231(4):286-298.

38. Fielding D, Oki M. Technologies for targeting the peripheral pulmonary nodule including robotics [published online ahead of print, 2020 February 26]. *Respirology*. 2020. https://doi.org/10.1111/resp.13791.
39. Lin AW, Trejos AL, Mohan S, et al. Electromagnetic navigation improves minimally invasive robot-assisted lung brachytherapy. *Comput Aided Surg*. 2008;13(2):114-123.
40. Avgousti S, Christoforou EG, Panayides AS, et al. Medical telerobotic systems: current status and future trends. *Biomed Eng Online*. 2016;15(1):96.
41. Xu X, Yu C, Qu J, et al. Imaging and clinical features of patients with 2019 novel coronavirus SARS-CoV-2. *Eur J Nucl Med Mol Imaging*. 2020;47(5):1275-1280.
42. Chung M, Bernheim A, Mei X, et al. CT imaging features of 2019 novel coronavirus (2019-nCoV). *Radiology*. 2020;295(1):202-207.
43. Dubinsky TJ, Shah H, Sonneborn R, et al. Correlation of B-lines on ultrasonography with interstitial lung disease on chest radiography and CT imaging. *Chest*. 2017;152(5):990-998.
44. Soldati G, Smargiassi A, Inchingolo R, et al. Proposal for international standardization of the use of lung ultrasound for patients with COVID-19: a simple, quantitative, reproducible method. *J Ultrasound Med*. 2020;39(7):1413-1419.
45. Yao XH, Li TY, He ZC, et al. A pathological report of three COVID-19 cases by minimally invasive autopsies [in Chinese]. *Zhonghua Bing Li Xue Za Zhi*. 2020;49(0):E009.
46. Wang D, Hu B, Hu C, et al. Clinical characteristics of 138 hospitalized patients with 2019 novel coronavirus-infected pneumonia in Wuhan, China. *JAMA* . 2020;323(11):1061-1069.
47. Li Q, Guan X, Wu P, et al. Early transmission dynamics in Wuhan, China, of novel coronavirus-infected pneumonia. *N Engl J Med*. 2020;382(13):1199-1207.
48. Wang HJ, Du SH, Yue X, et al. Review and prospect of pathological features of corona virus disease. *Fa Yi Xue Za Zhi*. 2020;36(1):16-20.
49. Tian S, Hu W, Niu L, et al. Pulmonary pathology of early-phase 2019 novel coronavirus (COVID-19) pneumonia in two patients with lung cancer. *J Thorac Oncol*. 2020;15(5):700-704.
50. Xu Z, Shi L, Wang Y, et al. Pathological findings of COVID-19 associated with acute respiratory distress syndrome. *Lancet Respir Med*. 2020;8(4):420-422.
51. Guan WJ, Liang WH, Zhao Y, et al. Comorbidity and its impact on 1590 patients with Covid-19 in China: a nationwide analysis. *Eur Respir J*. *Eur Respir J*. 2020;55(5):2000547.
52. Gudmundsson P, Rydberg E, Winter R, et al. Visually estimated left ventricular ejection fraction by echocardiography is closely correlated with formal quantitative methods. *Int J Cardiol*. 2005;101(2):209-212.
53. Vermeiren GL, Malbrain ML, Walpot JM. Cardiac ultrasonography in the critical care setting: a practical approach to asses cardiac function and preload for the "non-cardiologist.". *Anaesthesiol Intensive Ther*. 2015;47(spec no.):s89-s104.
54. van 't Hof AW, Schipper CW, Gerritsen JG, et al. Comparison of radionuclide angiography with three echocardiographic parameters of left ventricular function in patients after myocardial infarction. *Int J Card Imaging*. 1998;14(6):413-418.
55. Teijaro JR. The role of cytokine responses during influenza virus pathogenesis and potential therapeutic options. *Curr Top Microbiol Immunol*. 2015;386:3-22.
56. Shen J, Zhang CJP, Jiang B, et al. Artificial intelligence versus clinicians in disease diagnosis: systematic review. *JMIR Med Inform*. 2019;7(3):e10010.
57. Choi Y, Baek J, Park H, et al. A computer-aided diagnosis system using artificial intelligence for the diagnosis and characterization of thyroid nodules on ultrasound: initial clinical assessment. *Thyroid*. 2017;27(4):546-552.
58. Ma J, Wu F, Jiang T, et al. Cascade convolutional neural networks for automatic detection of thyroid nodules in ultrasound images. *Med Phys*. 2017;44(5):1678-1691.